iScience

CellPress
OPEN ACCESS

Article

IKKβ signaling mediates metabolic changes in the hypothalamus of a Huntington disease mouse model

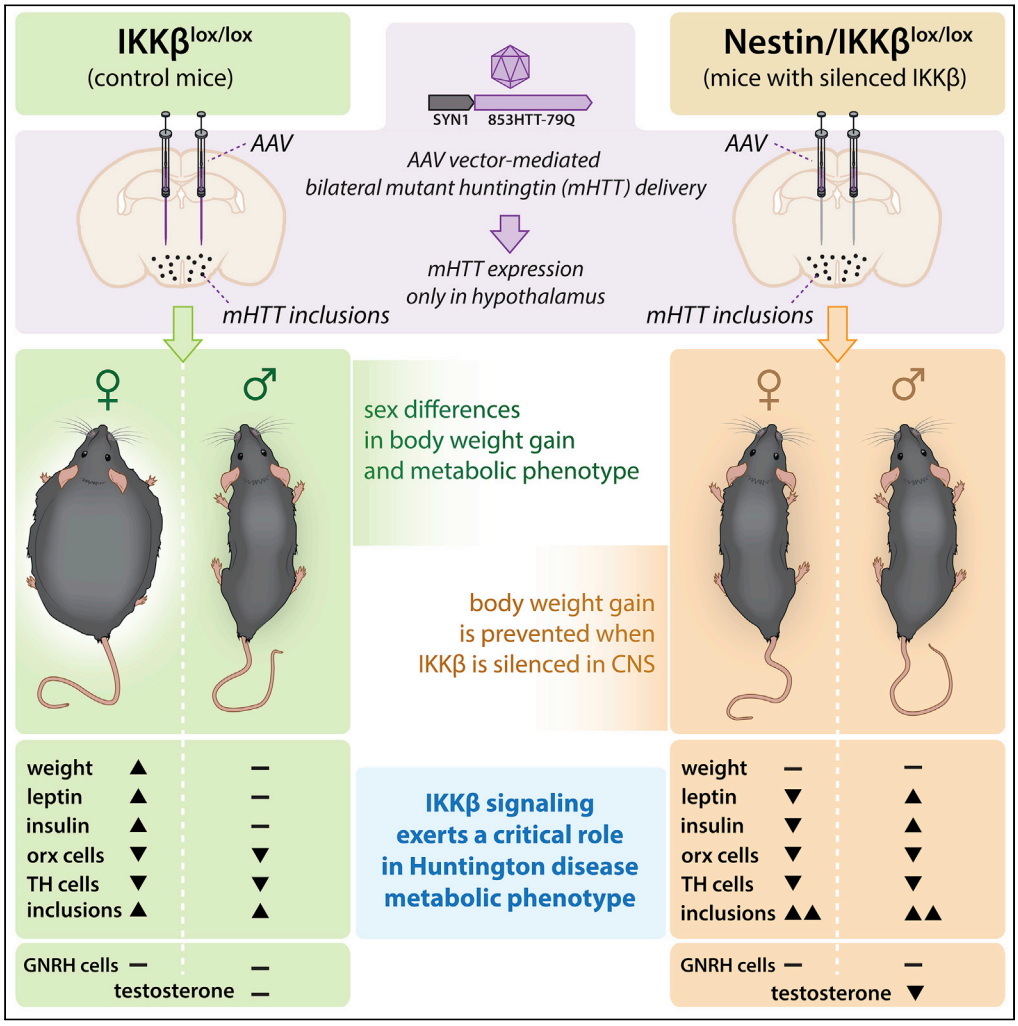

Rana Soylu-Kucharz, Ali Khoshnan, Åsa Petersén

rana.soylu_kucharz@med.lu.se

Highlights

Mutant huntingtin in the hypothalamus causes sex-specific metabolic imbalance

CNS-specific inactivation of the IKKβ pathway prevents the obese phenotype

IKKβ inactivation leads to an increased number of mutant huntingtin inclusions

IKKβ inactivation does not prevent orexin or A13 TH neuron loss

Soylu-Kucharz et al., iScience 25, 103771
February 18, 2022
https://doi.org/10.1016/j.isci.2022.103771

iScience

CellPress
OPEN ACCESS

Article

IKKβ signaling mediates metabolic changes in the hypothalamus of a Huntington disease mouse model

Rana Soylu-Kucharz,[1,3,*] Ali Khoshnan,[2] and Åsa Petersén[1]

SUMMARY

Huntington disease (HD) is a neurodegenerative disorder caused by a CAG repeat expansion in the huntingtin (*HTT*) gene. Metabolic changes are associated with HD progression, but underlying mechanisms are not fully known. As the IKKβ/NF-κB pathway is an essential regulator of metabolism, we investigated the involvement of IKKβ, the upstream activator of NF-κB in hypothalamus-specific HD metabolic changes. We expressed amyloidogenic N-terminal fragments of mutant HTT (mHTT) in the hypothalamus of mice with brain-specific ablation of IKKβ (Nestin/IKKβ$^{lox/lox}$) and control mice (IKKβ$^{lox/lox}$). We assessed effects on body weight, metabolic hormones, and hypothalamic neuropathology. Hypothalamic expression of mHTT led to an obese phenotype only in female mice. CNS-specific inactivation of IKKβ prohibited weight gain in females, which was independent of neuroprotection and microglial activation. Our study suggests that mHTT in the hypothalamus causes metabolic imbalance in a sex-specific fashion, and central inhibition of the IKKβ pathway attenuates the obese phenotype.

INTRODUCTION

Huntington disease (HD) is a fatal neurodegenerative disorder caused by a CAG repeat expansion in the huntingtin (HTT) gene (HDCRG, 1993). Although the clinical diagnosis is based on typical motor symptoms, affected individuals also suffer from early non-motor symptoms such as cognitive decline, psychiatric symptoms, and metabolic disturbances (Bates et al., 2015; Cheong et al., 2019). Metabolic changes in HD include weight loss despite adequate or even higher caloric intake (Aziz et al., 2008; Marder et al., 2009). A higher baseline body mass index (BMI) has been found to be a predictor of a slower disease progression in HD (van der Burg et al., 2017). Increased caloric intake has been correlated with increased phenoconversion in HD suggesting that metabolic changes may be a manifestation of HD severity (Marder et al., 2013). Hence, identifying the underlying mechanisms of metabolic changes in HD may increase our understanding of HD pathogenesis and progression as well as unravel new targets for therapeutic interventions to modify disease progression.

The hypothalamus is a master regulator of metabolism (Timper and Bruning, 2017; Cakir and Nillni, 2019). Imaging studies have identified hypothalamic changes in both prodromal and symptomatic HD patients (Douaud et al., 2006; Kassubek et al., 2004; Politis et al., 2008; Soneson et al., 2010). Analyses of postmortem hypothalamic tissue from HD cases and animal models (Cheong et al., 2019) showed loss of neuronal populations expressing orexin (hypocretin), oxytocin, and vasopressin, as well as altered metabolic pathways in several hypothalamic nuclei (Petersen et al., 2005; Gabery et al., 2010, 2015b; Baldo et al., 2019). Inactivation of mutant HTT (mHTT) selectively in the hypothalamus in female transgenic BACHD mouse model prevented development of a metabolic phenotype with obesity accompanied by leptin and insulin resistance (Gray et al., 2008). Similarly, local expression of mHTT in the hypothalamus using recombinant adeno-associated viral (rAAV) vectors in mice led to hyperphagic obesity with leptin and insulin resistance in normal chow diet-fed mice (Soylu-Kucharz et al., 2015, Hult et al., 2011). Transgene expression was present throughout the whole hypothalamus in these experiments (Hult et al., 2011). A number of studies selectively inactivating mHTT in specific metabolism regulating cell populations in mice expressing single-minded homolog 1 (Sim1), steroidogenic factor 1 (Sf1), or leptin receptor (LepR) showed no major effect on the BACHD mice metabolic phenotype (Baldo et al., 2014; Lundh et al., 2012; Cheong et al., 2020; Soylu-Kucharz et al., 2016). Hence, even though there is a causal link between hypothalamic expression of

[1]Translational Neuroendocrine Research Unit, Department of Experimental Medical Science, Lund University, BMC D11, 22184 Lund, Sweden

[2]California Institute of Technology, Pasadena, CA 91125, USA

[3]Lead contact

*Correspondence: rana.soylu_kucharz@med.lu.se

https://doi.org/10.1016/j.isci.2022.103771

mHTT and the development of metabolic imbalance in mice, the underlying cellular and molecular mechanisms are still not established.

The inhibition of κB kinase β/nuclear factor-κB (IKKβ/NF-κB) signaling pathway plays a significant role in obesity and overeating and is enriched in the hypothalamus (Zhang et al., 2008; Meng and Cai, 2011). Hyperphagia induced by a high-fat diet has been shown to activate IKKβ/NF-κB in the hypothalamus through increased ER stress, and suppression of IKKβ/NF-κB results in reduced food intake and normalized metabolic phenotype in mice (Zhang et al., 2008, 2017; Douglass et al., 2017). The IKKβ/NF-kB pathway is also activated by mHTT and has been associated with HD pathogenesis (Thompson et al., 2009; Atwal et al., 2011; Sarkar et al., 2011; Khoshnan et al., 2004; Becanovic et al., 2015; Trager et al., 2014). Several IKKβ silencing studies showed impaired clearance of mHTT and worsening HD pathological phenotypes *in vivo* and *in vitro* (Thompson et al., 2009; Khoshnan et al., 2009; Ochaba et al., 2019). *In vitro* studies using HeLa and osteosarcoma U2OS cells showed involvement of the IKK complex in the induction of autophagy (Criollo et al., 2010). The IKK complex directly interacted with Htt to phosphorylate Htt on S13 and S16 residues to promote activation of Htt clearance in PC12 and HEK-293 cell lines as well as in R6/2 and in a knockin HD animal models (Thompson et al., 2009; Khoshnan et al., 2004). *In vivo* studies silencing brain-specific IKKβ in the R6/1 mouse model showed a worsened behavioral phenotype with exacerbated neurodegeneration and activated microglial response in the R6/1 striatum (Ochaba et al., 2019).

However, it is not known whether the IKKβ/NF-κB pathway is involved in the development of HD metabolic imbalance. Based on the causal link of hypothalamic mHTT and the development of an obese phenotype, the data linking the hypothalamically enriched IKKβ/NF-κB signaling pathway with obesity and the known interactions of mHTT with this signaling pathway, we hypothesized that mHTT mediates metabolic imbalance via the IKKβ/NF-κB signaling pathway in the hypothalamus. In the present study, our aim was therefore to determine whether CNS-specific inactivation of the IKKβ/NF-κB pathway would prevent hypothalamic-induced metabolic changes induced by mHTT. We performed injections of rAAV vectors expressing mHTT into the hypothalamus of mice without IKKβ in the CNS (Nestin/IKKβ$^{lox/lox}$) and compared metabolic effects to control mice with the floxed allele of IKKβ (IKKβ$^{lox/lox}$).

RESULTS

Inhibition of the IKKβ pathway protects from hypothalamic mHTT-induced obesity in female mice

To assess the effects of mHTT expression on the development of a metabolic phenotype, we injected IKKβ$^{lox/lox}$ (homozygous for the floxed allele of IKKβ, control group) and Nestin/IKKβ$^{lox/lox}$ (expressing Cre-recombinase under nestin promotor) mice of both sexes with rAAV vectors expressing mHTT (AAV5-853HTT79Q vectors are referred to as HD elsewhere) in the hypothalamus. Consistent with our previous findings (Hult et al., 2011;Soylu-Kucharz et al., 2015; Baldo et al., 2013), expression of mHTT in female control mice led to an obese phenotype (Figures 1A and 1C). The body weight at 18 weeks post injection was significantly higher in the female IKKβ$^{lox/lox}$ + HD mice (n = 16 and mean = 55.6 g, SD = 10.2) compared to Nestin/IKKβ$^{lox/lox}$ + HD mice (n = 20 and mean = 40.6 g, SD = 9.3, $p < 0.0001$) and uninjected mice of the two genotypes (uninjected IKKβ$^{lox/lox}$: n = 15 and mean = 43.7 g, SD = 7.4, $p = 0.0026$; uninjected Nestin/IKKβ$^{lox/lox}$: n = 13 and mean = 37.1 g, SD = 9.8, $p < 0.0001$). Hence, inactivation of the IKKβ pathway in Nestin-expressing cells protected female mice from hypothalamic mHTT-induced obesity (Figure 1A). The brain-specific deletion of IKKβ did not affect the circulating insulin and leptin levels in mice (Meng and Cai, 2011). Therefore, in this study, we assessed the serum levels of insulin and leptin levels only in mice expressing mHTT in the hypothalamus. In line with the prevention of body weight gain, female Nestin/IKKβ$^{lox/lox}$ + HD mice displayed significantly lower serum levels of insulin and leptin than IKKβ$^{lox/lox}$ + HD mice (Figure 1D).

IKKβ did not affect the body weight in male mice with or without injections of AAV5-853HTT79Q as assessed up to 18 weeks post injection (Figures 1B and 1F). However, analyses of serum levels of insulin and leptin showed that even though there was no effect on body weight, levels of insulin and leptin were significantly elevated in male Nestin/IKKβ$^{lox/lox}$ + HD mice compared to IKKβ$^{lox/lox}$ + HD mice (Figures 1G and 1H). The two-way ANOVA analysis also showed that there were no significant differences in body weight between non-HD control groups at 18 weeks post injection time point for both females and males (Figure 1C; females, $p = 0.2474$ and Figure 1F; males, $p = 0.8796$).

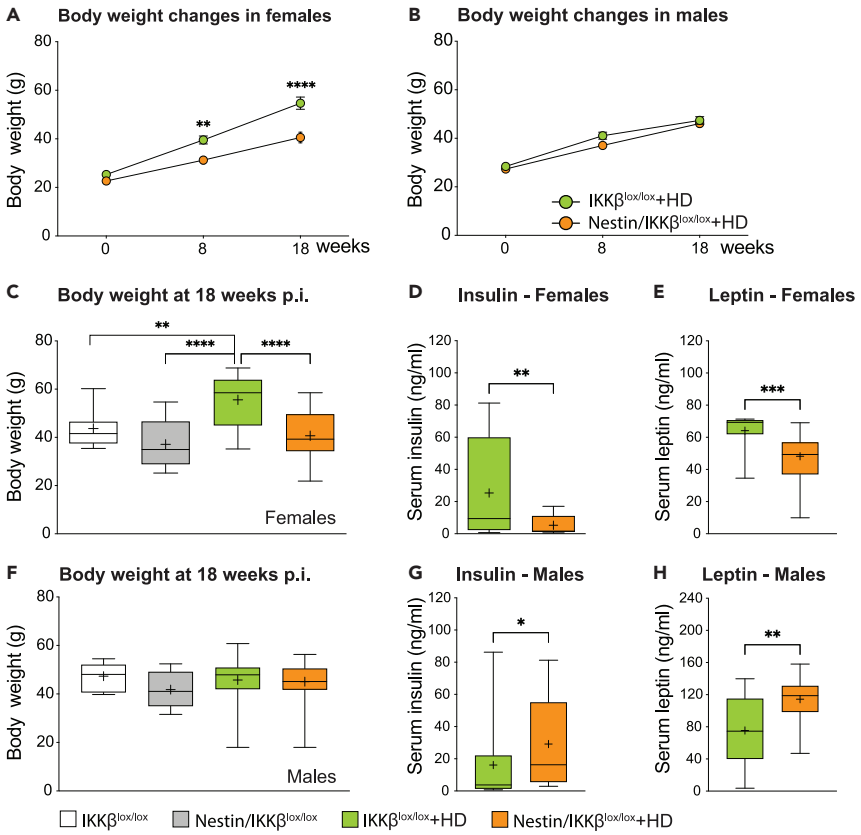

Figure 1. Inactivation of the IKKβpathway inhibits the development of obesityinduced by mHTT expression in the hypothalamus of female mice. IKKβ$^{lox/lox}$ and Nestin/IKKβ$^{lox/lox}$ mice were injected bilaterally into the hypothalamus with AAV-HTT853-79Q vectors and assessed using metabolic analyses

(A) Female IKKβ$^{lox/lox}$ mice develop increased body weight after hypothalamic injections of AAV5-HTT853-79Q vectors which is prevented in Nestin/IKKβ$^{lox/lox}$ + HD female mice (two-way repeated measures ANOVA, effect of time F (2, 62) = 8.920, p < 0.0001; effect of genotype F (1, 31) = 20.83, p < 0.0001; effect of genotype x time F (2, 62) = 8.920, p = 0.0004; followed by a Sidak's multiple comparisons test: p= 0.0026 at 8 weeks and p<0.0001at 18 weeks).

(B) Male IKKβ$^{lox/lox}$ and Nestin/IKKβ$^{lox/lox}$ mice do not develop obesity after AAV5-HTT853-79Q vector injections (two-way repeated measures ANOVA, effect of time F (2, 72) = 190.4, p < 0.0001; effect of genotype F (1, 36) = 2.359, P = 0.1333; effect of genotype x time F (2, 72) = 1.446, p = 0.2422, followed by a Sidak's multiple comparisons test).

(C) Body weight changes at 18 weeks post injection in females (one-way ANOVA, effect of treatment F (3, 60) = 11.69, p < 0.0001, followed by Sidak's multiple comparisons test, IKKβ$^{lox/lox}$ vs Nestin/IKKβ$^{lox/lox}$ p = 0.2474). Serum (D) insulin (two-tailed, unpaired t-test, n = 16/19, p = 0.0082) and (E) leptin (two-tailed, Mann Whitney test, n = 16/19, p = 0.0003) concentrations measured by ELISA in females at 18 weeks post injection.

(F) Body weight changes at 18 weeks post injection in males (one-way ANOVA, effect of treatment F (3, 55) = 0.7312, p = 0.5378 followed by Sidak'l's multiple comparisons test, IKKβ$^{lox/lox}$ vs Nestin/IKKβ$^{lox/lox}$ p = 0.8796). Serum (G) insulin (two-tailed, Mann Whitney test, n = 15/21, p = 0.0448) and (H) leptin (two-tailed, unpaired t-test, n = 15/21, p = 0.0023) assessments at 18 weeks. Data are represented as box and whisker plots (25–75 percentile (boxes), min to max (whiskers), median (horizontal line), mean (+)).

IKKβ is not involved in the mHTT-mediated loss of orexin and TH-positive cell populations in HD mice

The development of the metabolic phenotype in HD has been associated with expression of mHTT in the hypothalamus (Soylu-Kucharz et al., 2015, Hult et al., 2011). Here, we tested whether the rescue of the metabolic phenotype observed in Nestin/IKKβ$^{lox/lox}$ + HD mice was due to the preservation of metabolism-regulating neuronal populations known to be affected in HD (Cheong et al., 2019). In female mice, there was no benefit of IKKβ silencing as the number of orexin-positive cells in the lateral hypothalamus was comparable in IKKβ$^{lox/lox}$ + HD (cell loss ~64%) and Nestin/IKKβ$^{lox/lox}$ + HD groups (cell loss ~82%), and both groups had a significantly lower number of orexin cells compared to uninjected groups of female mice (Figures 2A and 2B). Male Nestin/IKKβ$^{lox/lox}$ + HD mice had significantly lower orexin and A13 TH-positive cells

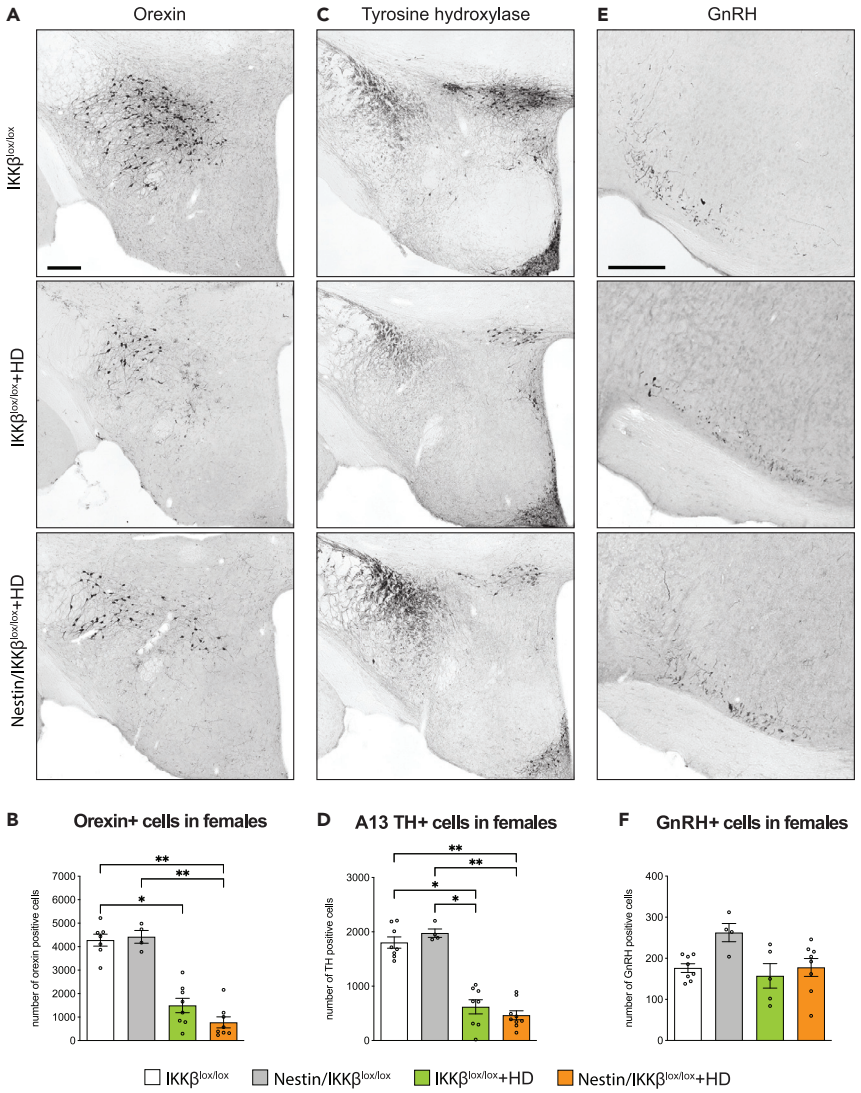

Figure 2. Quantitative analysis of the neuronal populations expressing orexin, TH in the A13 area, and GnRH in female mice at 18 week post injection of AAV-HTT853-79Q vectors

(A) Representative immunohistochemically stained sections show orexin immunopositive cells in the hypothalamus.

(B) Stereological analysis of orexin immunopositive cells in female mice at the 18 weeks time point (Kruskal-Wallis test followed by Dunn's multiple comparisons test p = 0.0002; n = 4-8/group).

(C) Representative photomicrographs show the A13 TH immunopositive cell population in the hypothalamus.

(D) Numbers of A13 TH-positive cells in the hypothalamus's zona incerta area (Kruskal-Wallis test followed by Dunn's multiple comparisons test p = 0.0001; n = 4-9/group).

(E) Representative photomicrographs illustrate the GnRH-positive cells in the anterior hypothalamic area of the hypothalamus.

(F) Stereological quantification of GnRH-positive cells in the anterior hypothalamic area (Kruskal-Wallis test followed by Dunn's multiple comparisons p = 0.0802; n = 4-8/group). Points on scatter graphs represent total cell count for individual mice, the lines are means, and the whiskers indicate ±SEM Scale bars represent 200 μm.

than IKKβ$^{lox/lox}$ + HD mice in the hypothalamus (FiguresS1A and S1B). The loss of A13 TH-positive cells was ~80% in Nestin/IKKβ$^{lox/lox}$ + HD and ~65% in IKKβ$^{lox/lox}$ + HD when compared to WT and Nestin/IKKβ$^{lox/lox}$ uninjected female mice (Figures 2C and 2D).

Reduced testosterone levels are associated with increased circulating levels of leptin and insulin, even in the absence of increased BMI (Pitteloud et al., 2005; Luukkaa et al., 1998). The hypothalamic-pituitary-gonadal

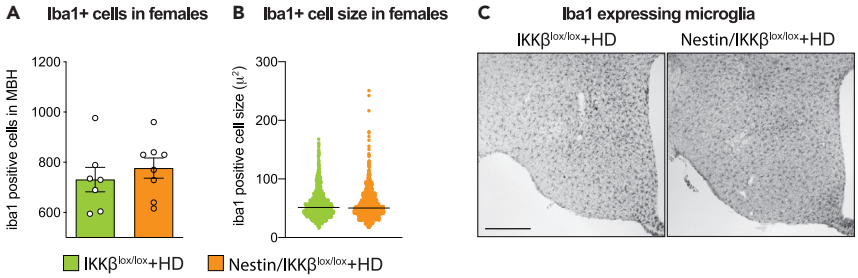

Figure 3. No effect of the IKKβ pathway on the degree of iba-1 positive cell activation at 18 weeks post injection in females

Stereological assessment of (A) the total number of iba-1 positive cells (two-tailed, unpaired t-test, n=7/8, p = 0.477) and (B) the size of Iba-1 positive cells (two-tailed, Mann-Whitney test, n=7/8 animals, n = 783/911 cells/genotype, p = 0.9601) in the mediobasal hypothalamus (MBH) 18 weeks after injections of AAV5-HTT853-79Q vectors in IKKβ$^{lox/lox}$ and Nestin/IKKβ$^{lox/lox}$ mice. In (A), data are represented as scatter dot plots, and bars represent mean ± SEM, and in (B), data are represented as scatter dot plots, and lines represent median.

(HPG) axis, which regulates testosterone production, is altered in HD (Soylu-Kucharz et al., 2016; Markianos et al., 2005; Bird et al., 1976; Kalliolia et al., 2015; Saleh et al., 2009; Van Raamsdonk et al., 2007b; Papalexi et al., 2005; Petersen and Bjorkqvist, 2006). The number of GnRH-positive cells was comparable (Figures 2F and S1C); however, the total circulating level of testosterone was diminished in Nestin/IKKβ$^{lox/lox}$ + HD male mice by 60% compared to IKKβ$^{lox/lox}$ + HD male mice expressing mHTT in the hypothalamus (Figure S1D).

The number and size of Iba-1 positive microglial cells were comparable in the mediobasal hypothalamus

Given that IKKβ is one of the mediators of microglial activation and energy balance (Karin, 1999; Liu et al., 2017), we investigated whether protection from hypothalamic mHTT-induced obesity in Nestin/IKKβ$^{lox/lox}$ female mice was due to alteration in microglial activation. Nonetheless, the number and size of Iba1-positive cells in the mediobasal hypothalamus of both IKKβ$^{lox/lox}$ + HD and Nestin/IKKβ$^{lox/lox}$ + HD female mice were comparable (Figures 3A–3C).

Nestin/IKKβ$^{lox/lox}$ + HD female mice display an increased number of small-sized inclusions of mHTT

Reduction of IKKβ activity decreases the cleavage of both WT and mHTT and prevents the accumulation of mHTT inclusions (Khoshnan et al., 2009; Thompson et al., 2009). IKKβ silencing studies also showed impaired clearance of mHTT and worsening HD pathological phenotypes *in vivo* and vitro (Thompson et al., 2009; Khoshnan et al., 2009). In our model, mutant HTT was expressed throughout the hypothalamic region (Figure S2) and inclusions were increased in Nestin/IKKβ$^{lox/lox}$ + HD compared to IKKβ$^{lox/lox}$ + HD in both females and males (Figures 4A–4C). The small size inclusions were responsible for the increase, as the number of medium or large size inclusions were similar between IKKβ$^{lox/lox}$ + HD and Nestin/IKKβ$^{lox/lox}$ + HD groups (Figures 4D–4F). Altogether, these results show the increase in inclusion formation correlates with previous reports on IKKβ silencing in HD (Criollo et al., 2010; Khoshnan et al., 2009; Ochaba et al., 2019).

DISCUSSION

The hypothalamus plays a key role in the regulation of metabolism. In HD, both individuals with the mHTT gene and a number of animal models of the disease develop changes in the metabolism. Hypothalamic pathology is present early in the course of HD and is also recapitulated in the animal models (Gabery et al., 2015a, 2015b(Cheong et al., 2019)). Previous work has established a causal link between expression of mHTT in the hypothalamus and the development of a metabolic phenotype in mice (Hult et al., 2011). However, the underlying cellular or molecular mechanisms are not known. A potential link between pathological effects of mHTT in the hypothalamus and hypothalamic induction of obesity was provided by the hypothalamus-enriched IKKβ/NF-κB signaling system, which has been implicated both in the pathogenesis of obesity and HD (Cai and Khor, 2019; Khoshnan and Patterson, 2011; Ochaba et al., 2019). Here, we therefore tested whether CNS-specific inactivation of IKKβ had an effect on hypothalamic mHTT-induced

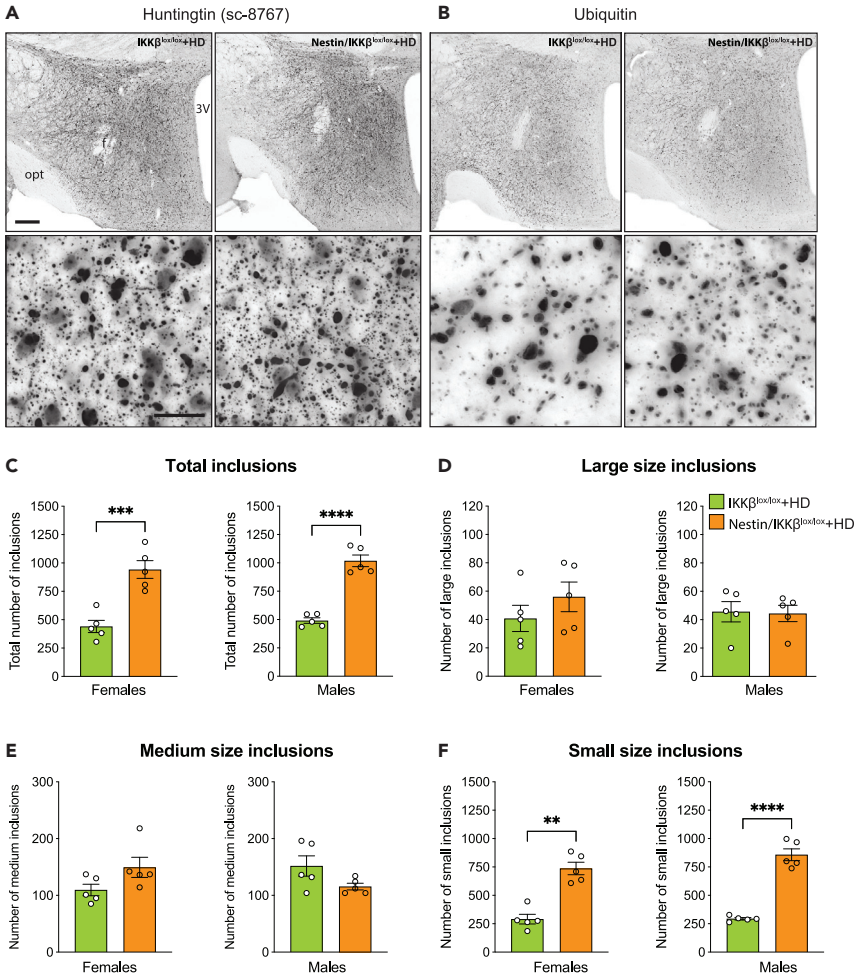

Figure 4. Inactivation of the IKKβ pathway leads to increased numbers of huntingtin inclusions in the hypothalamus

Representative photomicrographs of sections processed for immunohistochemistry for (A) huntingtin (using the sc-8767 antibody) and (B) ubiquitin demonstrating the formation of inclusions in the hypothalamus after injections of AAV-HTT853-79Q vectors in IKKβ$^{lox/lox}$ and Nestin/IKKβ$^{lox/lox}$ mice. Stereological quantification of sections processed with the huntingtin antibody shows (C) the total number of inclusions (Females: two-tailed, Mann-Whitney test, n = 5/group, p = 0.0008; Males: two-tailed, Mann-Whitney test, n = 5/group, p < 0.0001), (D) large-sized inclusions (Females: two-tailed, Mann-Whitney test, n = 5/group, p = 0.3095; Males: two-tailed, unpaired t-test, n = 5/group, p = 0.8992), (E) medium-sized inclusions (Females: two-tailed, unpaired t-test, n = 5/group, p = 0.0635); Males: two-tailed, unpaired t-test, n = =5/group, p = 0.0911), and (F) small-sized inclusions (Females: two-tailed, Mann-Whitney test, n = 5/group, p = 0.0079; Males: two-tailed, unpaired t-test, n = 5/group, p < 0.0001) inclusions in female and male mice at 18 weeks post injection. Points on scatter graphs represent total inclusion count for individual mice, the lines are means, and the whiskers indicate ±SEM Scale bars represent 200 and 25 μm on lower and higher magnifications, respectively.

metabolic imbalance and found that it indeed prevented the development of obesity in female mice. Previous studies have shown that a high-fat diet is important for the effect of IKKβ/NF-κB signaling to induce obesity in mice (Zhang et al., 2008). Here, we show that inhibition of this pathway is also protective against obesity-induced under normalchow diet feeding by expression of pathogenic mHTT in the hypothalamus.

In HD, both the wild-type HTT protein and the mHTT protein are expressed throughout the body (Cattaneo et al., 2005). Yet, the disease is associated with selective regional pathology and a defined set of clinical symptoms. Therefore, it is essential to identify the causal relationships between specific regional pathology and the different symptoms and signs of the disease to advance the understanding of the development of the disease and unravel new targets for therapeutic intervention. By taking advantage of AAV vectors, we

examined the effects of mHTT specifically in the hypothalamus while excluding its effects on other brain regions and the periphery. With the viral vector approach, we have previously revealed a causal link between hypothalamic huntingtin expression and metabolic disturbances (Hult et al., 2011). The BACHD mouse model exhibits increased body weight, and hypothalamic mHTT silencing can prohibit the development of obese phenotype (Hult et al., 2011;Gray et al., 2008). In parallel, the selective expression of mHTT fragment in the hypothalamus recapitulates BACHD metabolic alterations (Hult et al., 2011). However, how mHTT expression in the hypothalamus leads to metabolic imbalance remained unknown. We have previously explored several potential cellular mechanisms using a Cre-lox system-based crossbreeding approach to identify the specific metabolic pathways involved. Silencing of mHTT in single-minded homolog 1 (Sim1), steroidogenic factor 1 (Sf1), and leptin receptor (LepR)-expressing neurons of mice showed no effect or only a sex-specific minor effect on the BACHD mice metabolic phenotype (Baldo et al., 2014; Lundh et al., 2012; Cheong et al., 2020; Soylu-Kucharz et al., 2016). The IKKβ/NF-κB pathway has been implicated in HD pathogenesis (Khoshnan and Patterson, 2011), but it has not been previously investigated in the context of HD metabolic and hypothalamic alterations. Here, we show for the first time that inactivation of the IKKβ, a key regulator of the NF-κB pathway, prevents the development of metabolic abnormalities induced by mHTT in the hypothalamus.

Formation of huntingtin inclusions is a hallmark of HD, and the IKKβ/NF-kB pathway has been shown to be involved in the degradation of mHTT in a complex fashion (Thompson et al., 2009; Atwal et al., 2011; Sarkar et al., 2011; Khoshnan et al., 2004; Becanovic et al., 2015; Trager et al., 2014). IKKβ activity affects phosphorylation of Htt at Ser13 and Ser16 residues, yielding in increase clearance of HTT and reduced cellular toxicity (Thompson et al., 2009). In the R6/1 mouse model of HD, brain-specific deletion of IKKβ worsened the behavioral phenotype and led to exacerbated neurodegeneration with an activated microglial response in the striatum (Ochaba et al., 2019). Furthermore, an SNP in the HTT promoter has been shown to affect NF-kB binding and age of onset in a cohort of patients with HD (Becanovic et al., 2015). In line with previous studies, CNS-specific silencing of IKKβ was associated with an increase in the number of hypothalamic mHTT inclusions, in particular of the smallest size. Previous studies showed that not only mHTT but also wild-type HTT might have an effect in regulating metabolism. The body weights of YAC18 mice were significantly higher compared with YAC128 mice (Pouladi et al., 2010). We also showed that expression of the wild-type HTT fragments with 18Q in the hypothalamus leads to delayed and slower body weight gain without any formation of inclusions immunopositive for ubiquitin in the 18Q group (Soylu-Kucharz et al., 2015). Altogether, while these results indicate that an increase in inclusion formation correlates with silenced IKK activation, the increase in inclusion number is less likely to be associated with inhibition of hyperphagia induced by mHTT.

An obese phenotype can develop due to increased caloric intake, decreased activity, metabolic rate, or a combination of these factors. Previously, we demonstrated that the obese phenotype caused by hypothalamic mHTT expression was due to hyperphagia as general motor activity and basal metabolic rate were unaltered in these mice (Hult et al., 2011). The mice in this study were housed in a separate animal unit that lacks behavior testing platforms and limiting the number of in-house cages. Therefore, we were not able to re-test basic parameters such as food intake and locomotor activity. However, as we have previously shown that the obese phenotype was caused by increased food intake, we speculate that the silencing of the IKKβ expression prohibited hyperphagia-induced obesity in HD mice. The lateral hypothalamus orexin and A13 TH neuronal populations are involved in metabolism regulation (Adeghate et al., 2020; Shi et al., 2013) and they are affected in HD (Petersen et al., 2005; Gabery et al., 2010; Hult et al., 2011; Soylu-Kucharz et al., 2015). As the inactivation of the IKKβ signaling did not affect the preservation of these cells, we can speculate that orexin and A13 TH neuropathology are not the central cell populations responsible for the development of HD bodyweight alterations.

Clinical HD is associated with progressive weight loss, despite adequate or even higher caloric intake. A higher BMI has been found to be a predictor of slower clinical decline independent of mutant HTT CAG repeat size (van der Burg et al., 2017). In this study, diet type was not addressed, as the BMI is a value that does not distinguish between fat and lean mass, it remains unknown whether a higher baseline BMI is due to an increase in fat mass or lean mass. In previous work, we aimed to understand whether an increase in fat mass can play a neuroprotective role in R6/2 mice by crossing R6/2 mice with ob/ob mice and found that higher BMI due to an increase in fat mass did not improve HD phenotype (Sjogren et al., 2019). Others reported that the R6/2 mice exposed to HFD showed a significantly higher body weight

gain than WT controls, but the HFD-induced bodyweight increase had no effect on the late-stage weight loss phenotype and longevity (Fain et al., 2001). Marder et al. found that higher caloric intake was correlated with increased phenoconversion, further emphasizing that the relationship between a higher BMI and slower disease progression might not be due to increased fat mass rather an increase in muscle mass (Marder et al., 2013). In contrast to studies addressing BMI and diet type, the expression of mutant HTT fragments in the hypothalamus leads to hyperphagic obesity in wild-type mice fed on a standard chow diet (Baldo et al., 2013; Hult et al., 2011; Soylu-Kucharz et al., 2015). As increased caloric intake has also been reported in clinical HD, our experimental approach helps to understand how hypothalamic mutant HTT expression leads to increased food intake in standard chow-fed animals.

The present study shows that the effect on metabolism induced by mHTT expression in the hypothalamus is sex dependent as only female mice developed the severe metabolic phenotype with obesity. Gender differences may play a role in HD as the severity and rate of the motor symptoms progression has been suggested to be faster in women than men with HD (Zielonka et al., 2013; Zielonka et al., 2018; Zielonka and Stawinska-Witoszynska, 2020). Previous studies indicated that sex also affects HD metabolic and behavioral manifestation in animal models (Soylu-Kucharz et al., 2016; Dorner et al., 2007; Sjogren et al., 2019). BACHD females have a higher degree of weight gain than BACHD males relative to their WT littermates, and BACHD motor deficits were more severe in females than males (Van Raamsdonk et al., 2007a;Menalled et al., 2009). In line with this, the obese phenotype caused by hypothalamus-specific mHTT overexpression leads to reduced locomotor activity suggesting a potential contribution of the metabolic phenotype to motor deficits (Hult et al., 2011). It would be interesting to further examine if hypothalamic-specific mHTT expression and the accompanying metabolic phenotype further contributes to disease progression including to neuropathology in other areas of the brain (Soylu-Kucharz et al., 2018,(Dickson, 2022)).

The Nestin-Cre mouse model is commonly employed in studies to drive deletions in the nervous system. The expression pattern of Cre-recombinase in the NestinCre mice brain was shown by using *in situ* hybridization, and neuronal Cre recombinase expression was widespread in the adult brain and in a small portion of astroglial cells (Giusti et al., 2014). Insufficient expression of Cre-recombinase has been shown in the embryonic and early postnatal stages of Nestin-Cre mice. However, recombination was shown to be reaching nearly 100% in neural cells during perinatal development (Liang et al., 2012). In our study, we injected mice with a viral vector at the earliest 8 weeks of age when the Cre-mediated excision of flanking DNA sequence was completed. Therefore, we can conclude that expression of mHTT occurs after complete IKKβ silencing in neurons. Furthermore, we employed an AAV vector that expresses mHTT fragment under human synapsin-1 promoter to drive mHTT expression in neuronal cells.

The HD metabolic phenotype does not appear to be associated with the genetic strain background of HD animal models. BACHD and YAC128 mice exhibit obese phenotypes on both the FVB/N and the B6 background (Menalled et al., 2009; Pouladi et al., 2012; Van Raamsdonk et al., 2007a; Gray et al., 2008). Using the viral vector approach to selectively express mHTT in specific brain regions, we found that the expression of hypothalamic mHTT in female control mice from both the FVB/N and B6 strains developed comparable metabolic phenotypes (Hult et al., 2011). The expression of mHTT in the hypothalamus of male mice from the B6 strain used in this study did not affect body weight, although male Nestin/IKKβ$^{lox/lox}$ + HD mice displayed high serum leptin and insulin levels. As testosterone deficiency is associated with metabolic syndrome exemplified by increased circulating leptin levels and insulin resistance, it is possible that the increase in serum leptin and insulin levels could be due to reduced circulating testosterone levels in Nestin/IKKβ$^{lox/lox}$ + HD mice. However, further studies are required to investigate the role of testosterone deficiency on circulating metabolic factors in HD. Furthermore, the effect of hypothalamic mHTT on the metabolism has not been investigated in male mice from the FVB/N stain. Even though we cannot be certain that the reduced metabolic phenotype in males in the present study was only due to an effect of sex, previous studies on transgenic HD animal models indicate that strain has no major impact on the development of the metabolic phenotype.

In conclusion, our study shows that hypothalamic expression of mHTT leads to a metabolic imbalance in a sex-specific fashion. The metabolic phenotype induced by the mHTT in female mice is prevented by IKKβ inactivation and is independent of orexin and TH neuroprotection and microglial activation. The mechanistic explanation for the contribution of metabolic defects to HD progression and cachexia is a long-standing question. It is now known that there are strong associations between metabolic dysfunction and

neurodegeneration, especially for aging disorders such as Alzheimer, Parkinson, and Huntington diseases (Procaccini et al., 2016). Therefore, metabolic manipulations have also been considered as a possible therapeutic tool for several neurodegenerative diseases, including HD (Walker and Raymond, 2004; Duan et al., 2003; Procaccini et al., 2016). Interestingly, the IKK-β pathway in the hypothalamus has also been shown to be a key for the advancement of aging in mice (Zhang et al., 2013) and aging is thought to be involved in HD pathogenesis (Machiela et al., 2020; Machiela and Southwell, 2020). Given that the wild-type HTT also has a role in regulating metabolism, as it has been shown by body weight gain phenotype in YAC18 mice (Pouladi et al., 2010) and by using hypothalamic expression of HTT fragments with 18Q in mice (Soylu-Kucharz et al., 2015; Baldo et al., 2013), the IKK-β pathway has the potential to induce accelerated aging in HD by linking HTT clearance, metabolism alterations, and aging processes. In line with this, our data implicate the IKKβ pathway as a key regulator of metabolic imbalance induced by mHTT in the hypothalamus. It is therefore important to further elucidate the role of this pathway in HD pathogenesis in studies aiming at achieving disease-modifying metabolic effect in future therapeutic developments.

Limitations of the study

Although we showed that silencing of the IKKβ pathway is protective against mHTT-induced weight gain, this study lacks detailed metabolic profiling that would allow determination of the direct effect of this pathway on parameters such as food intake, energy expenditure, and physical activity.

STAR★METHODS

Detailed methods are provided in the online version of this paper and include the following:

- KEY RESOURCES TABLE
- RESOURCE AVAILABILITY
  - Lead contact
  - Materials availability
  - Data and code availability
- EXPERIMENTAL MODEL AND SUBJECT DETAILS
  - Animals
  - Adeno-associated viral vectors
- METHOD DETAILS
  - Viral vector injections
  - Perfusion and serum collection
  - Metabolic tests
  - Immunohistochemistry
  - Stereological analyses
- QUANTIFICATION AND STATISTICAL ANALYSIS

SUPPLEMENTAL INFORMATION

Supplemental information can be found online at https://doi.org/10.1016/j.isci.2022.103771

ACKNOWLEDGMENTS

This work was supported by grants from the Swedish Medical Research Council (grant numbers 2013/03537 and 2018/02559), the Province of Skåne State Grants (ALF) as well as the Knut and Alice Wallenberg Foundation (# 2019.0467) to ÅP. ÅP is a Wallenberg Clinical Scholar (Knut and Alice Wallenberg Foundation # 2019.0467). RSK was supported by the Swedish Society for Medical Research Fellowship. We are grateful for the excellent technical assistance provided by Björn Anzelius, Anneli Josefsson, Ulla Samuelsson, Ulrika Sparrhult-Bjork, and Krzysztof Kucharz for his help with the illustrations.

AUTHOR CONTRIBUTIONS

RS, ÅP, and AK conceived and designed the experiments. RSK performed the experiments. RSK and ÅP analyzed the data. RSK and ÅP wrote the first draft of the manuscript. All authors were involved in editing the manuscript and approved the final version.

DECLARATION OF INTERESTS

The authors declare no competing interests.

INCULISION AND DIVERSITY

We worked to ensure sex balance in the selection of non-human subjects.

Received: July 8, 2021
Revised: November 16, 2021
Accepted: January 11, 2022
Published: February 18, 2022

REFERENCES

Adeghate, E., Lotfy, M., D'souza, C., Alseiari, S.M., Alsaadi, A.A., and Qahtan, S.A. (2020). Hypocretin/orexin modulates body weight and the metabolism of glucose and insulin. Diabetes Metab. Res. Rev. *36*, e3229.

Atwal, R.S., Desmond, C.R., Caron, N., Maiuri, T., Xia, J., Sipione, S., and Truant, R. (2011). Kinase inhibitors modulate huntingtin cell localization and toxicity. Nat. Chem. Biol. *7*, 453–460.

Aziz, N.A., Van Der Burg, J.M., Landwehrmeyer, G.B., Brundin, P., Stijnen, T., EHDI Study Group, and Roos, R.A. (2008). Weight loss in Huntington disease increases with higher CAG repeat. Neurology *71*, 1506–1513.

Baldo, B., Cheong, R.Y., and Petersen, A. (2014). Effects of deletion of mutant huntingtin in steroidogenic factor 1 neurons on the psychiatric and metabolic phenotype in the BACHD mouse model of Huntington disease. PLoS One *9*, e107691.

Baldo, B., Gabery, S., Soylu-Kucharz, R., Cheong, R.Y., Henningsen, J.B., Englund, E., Mclean, C., Kirik, D., Halliday, G., and Petersen, A. (2019). SIRT1 is increased in affected brain regions and hypothalamic metabolic pathways are altered in Huntington disease. Neuropathol. Appl. Neurobiol. *45*, 361–379.

Baldo, B., Soylu, R., and Petersen, A. (2013). Maintenance of basal levels of autophagy in Huntington's disease mouse models displaying metabolic dysfunction. PloS one *8*, e83050.

Bates, G.P., Dorsey, R., Gusella, J.F., Hayden, M.R., Kay, C., Leavitt, B.R., Nance, M., Ross, C.A., Scahill, R.I., Wetzel, R., et al. (2015). Huntington disease. Nat. Rev. Dis. Primers *1*, 15005.

Becanovic, K., Norremolle, A., Neal, S.J., Kay, C., Collins, J.A., Arenillas, D., Lilja, T., Gaudenzi, G., Manoharan, S., Doty, C.N., et al. (2015). A SNP in the HTT promoter alters NF-kappaB binding and is a bidirectional genetic modifier of Huntington disease. Nat. Neurosci. *18*, 807–816.

Betz, U.A., Vosshenrich, C.A., Rajewsky, K., and Muller, W. (1996). Bypass of lethality with mosaic mice generated by Cre-loxP-mediated recombination. Curr. Biol. *6*, 1307–1316.

Bird, E.D., Chiappa, S.A., and Fink, G. (1976). Brain immunoreactive gonadotropin-releasing hormone in Huntington's chorea and in non-choreic subjects. Nature *260*, 536–538.

Cai, D., and Khor, S. (2019). Hypothalamic microinflammation" paradigm in aging and metabolic diseases. Cell Metab *30*, 19–35.

Cakir, I., and Nillni, E.A. (2019). Endoplasmic reticulum stress, the hypothalamus, and energy balance. Trends Endocrinol.Metab. *30*, 163–176.

Cattaneo, E., Zuccato, C., and Tartari, M. (2005). Normal huntingtin function: an alternative approach to Huntington's disease. Nat. Rev. Neurosci. *6*, 919–930.

Chen, L.W., Egan, L., Li, Z.W., Greten, F.R., Kagnoff, M.F., and Karin, M. (2003). The two faces of IKK and NF-kappaB inhibition: prevention of systemic inflammation but increased local injury following intestinal ischemia-reperfusion. Nat. Med. *9*, 575–581.

Cheong, R.Y., Gabery, S., and Petersen, A. (2019). The role of hypothalamic pathology for non-motor features of huntington's disease. J. Huntingtons Dis. *8*, 375–391.

Cheong, R.Y., Tonetto, S., Von Horsten, S., and Petersen, A. (2020). Imbalance of the oxytocin-vasopressin system contributes to the neuropsychiatric phenotype in the BACHD mouse model of Huntington disease. Psychoneuroendocrinology *119*, 104773.

Criollo, A., Senovilla, L., Authier, H., Maiuri, M.C., Morselli, E., Vitale, I., Kepp, O., Tasdemir, E., Galluzzi, L., Shen, S., et al. (2010). The IKK complex contributes to the induction of autophagy. EMBO J. *29*, 619–631.

Dickson, Elna, et al. (2022). Hypothalamic expression of huntingtin causes distinct metabolic changes in Huntington's disease mice. Molecular Metabolism. https://doi.org/10.1016/j.molmet.2022.101439.

Dorner, J.L., Miller, B.R., Barton, S.J., Brock, T.J., and Rebec, G.V. (2007). Sex differences in behavior and striatal ascorbate release in the 140 CAG knock-in mouse model of Huntington's disease. Behav. Brain Res. *178*, 90–97.

Douaud, G., Gaura, V., Ribeiro, M.J., Lethimonnier, F., Maroy, R., Verny, C., Krystkowiak, P., Damier, P., Bachoud-Levi, A.C., Hantraye, P., and Remy, P. (2006). Distribution of grey matter atrophy in Huntington's disease patients: a combined ROI-based and voxel-based morphometric study. Neuroimage *32*, 1562–1575.

Douglass, J.D., Dorfman, M.D., Fasnacht, R., Shaffer, L.D., and Thaler, J.P. (2017). Astrocyte IKKbeta/NF-kappaB signaling is required for diet-induced obesity and hypothalamic inflammation. Mol. Metab. *6*, 366–373.

Duan, W., Guo, Z., Jiang, H., Ware, M., Li, X.J., and Mattson, M.P. (2003). Dietary restriction normalizes glucose metabolism and BDNF levels, slows disease progression, and increases survival in huntingtin mutant mice. Proc. Natl. Acad. Sci. U S A *100*, 2911–2916.

Fain, J.N., Del Mar, N.A., Meade, C.A., Reiner, A., and Goldowitz, D. (2001). Abnormalities in the functioning of adipocytes from R6/2 mice that are transgenic for the Huntington's disease mutation. Hum. Mol. Genet. *10*, 145–152.

Franklin, K.P., and Paxinos, G. (2008). The Mouse Brain in Stereotaxic Coordinates (Academic Press).

Gabery, S., Georgiou-Karistianis, N., Lundh, S.H., Cheong, R.Y., Churchyard, A., Chua, P., Stout, J.C., Egan, G.F., Kirik, D., and Petersen, A. (2015a). Volumetric analysis of the hypothalamus in huntington disease using 3T MRI: the IMAGE-HD study. PloS one *10*, e0117593.

Gabery, S., Halliday, G., Kirik, D., Englund, E., and Petersen, A. (2015b). Selective loss of oxytocin and vasopressin in the hypothalamus in early Huntington disease: a case study. Neuropathol. Appl. Neurobiol. *41*, 843–848.

Gabery, S., Murphy, K., Schultz, K., Loy, C.T., Mccusker, E., Kirik, D., Halliday, G., and Petersen, A. (2010). Changes in key hypothalamic neuropeptide populations in Huntington disease revealed by neuropathological analyses. Acta neuropathologica *120*, 777–788.

Giusti, S.A., Vercelli, C.A., Vogl, A.M., Kolarz, A.W., Pino, N.S., Deussing, J.M., and Refojo, D. (2014). Behavioral phenotyping of Nestin-Cre mice: implications for genetic mouse models of psychiatric disorders. J. Psychiatr. Res. *55*, 87–95.

Gray, M., Shirasaki, D.I., Cepeda, C., Andre, V.M., Wilburn, B., Lu, X.H., Tao, J., Yamazaki, I., Li, S.H., Sun, Y.E., et al. (2008). Full-length human mutant huntingtin with a stable polyglutamine repeat can elicit progressive and selective neuropathogenesis in BACHD mice. J. Neurosci. *28*, 6182–6195.

Gundersen, H.J., Bagger, P., Bendtsen, T.F., Evans, S.M., Korbo, L., Marcussen, N., Moller, A., Nielsen, K., Nyengaard, J.R., Pakkenberg, B., et al. (1988). The new stereological tools: disector, fractionator, nucleator and point sampled intercepts and their use in pathological research and diagnosis. APMIS *96*, 857–881.

HDCRG (1993). A novel gene containing a trinucleotide repeat that is expanded and unstable on Huntington's disease chromosomes. The Huntington's Disease Collaborative Research Group. Cell *72*, 971–983.

Hult, S., Soylu, R., Bjorklund, T., Belgardt, B.F., Mauer, J., Bruning, J.C., Kirik, D., and Petersen, A. (2011). Mutant huntingtin causes metabolic

imbalance by disruption of hypothalamic neurocircuits. Cell Metab *13*, 428–439.

Kalliolia, E., Silajdzic, E., Nambron, R., Costelloe, S.J., Martin, N.G., Hill, N.R., Frost, C., Watt, H.C., Hindmarsh, P., Bjorkqvist, M., and Warner, T.T. (2015). A 24-hour study of the hypothalamo-pituitary axes in huntington's disease. PLoS One *10*, e0138848.

Karin, M. (1999). How NF-kappaB is activated: the role of the IkappaB kinase (IKK) complex. Oncogene *18*, 6867–6874.

Kassubek, J., Gaus, W., and Landwehrmeyer, G.B. (2004). Evidence for more widespread cerebral pathology in early HD: an MRI-based morphometric analysis. Neurology *62*, 523–524.

Khoshnan, A., Ko, J., Tescu, S., Brundin, P., and Patterson, P.H. (2009). IKKalpha and IKKbeta regulation of DNA damage-induced cleavage of huntingtin. PLoS One *4*, e5768.

Khoshnan, A., Ko, J., Watkin, E.E., Paige, L.A., Reinhart, P.H., and Patterson, P.H. (2004). Activation of the IkappaB kinase complex and nuclear factor-kappaB contributes to mutant huntingtin neurotoxicity. J. Neurosci. *24*, 7999–8008.

Khoshnan, A., and Patterson, P.H. (2011). The role of IkappaB kinase complex in the neurobiology of Huntington's disease. Neurobiol. Dis. *43*, 305–311.

Li, Z.W., Omori, S.A., Labuda, T., Karin, M., and Rickert, R.C. (2003). IKK beta is required for peripheral B cell survival and proliferation. J. Immunol. *170*, 4630–4637.

Liang, H., Hippenmeyer, S., and Ghashghaei, H.T. (2012). A Nestin-cre transgenic mouse is insufficient for recombination in early embryonic neural progenitors. Biol. Open *1*, 1200–1203.

Liu, T., Zhang, L., Joo, D., and Sun, S.C. (2017). NF-kappaB signaling in inflammation. Signal Transduct. Target. Ther. *2*, 17023.

Lundh, S.H., Soylu, R., and Petersen, A. (2012). Expression of mutant huntingtin in leptin receptor-expressing neurons does not control the metabolic and psychiatric phenotype of the BACHD mouse. PLoS One *7*, e51168.

Luukkaa, V., Pesonen, U., Huhtaniemi, I., Lehtonen, A., Tilvis, R., Tuomilehto, J., Koulu, M., and Huupponen, R. (1998). Inverse correlation between serum testosterone and leptin in men. J. Clin. Endocrinol. Metab. *83*, 3243–3246.

Machiela, E., Jeloka, R., Caron, N.S., Mehta, S., Schmidt, M.E., Baddeley, H.J.E., Tom, C.M., Polturi, N., Xie, Y., Mattis, V.B., et al. (2020). The interaction of aging and cellular stress contributes to pathogenesis in mouse and human huntington disease neurons. Front Aging Neurosci. *12*, 524369.

Machiela, E., and Southwell, A.L. (2020). Biological aging and the cellular pathogenesis of huntington's disease. J. Huntingtons Dis. *9*, 115–128.

Marder, K., Gu, Y., Eberly, S., Tanner, C.M., Scarmeas, N., Oakes, D., Shoulson, I., and Huntington Study Group, P.I. (2013). Relationship of Mediterranean diet and caloric intake to phenoconversion in Huntington disease. JAMA Neurol. *70*, 1382–1388.

Marder, K., Zhao, H., Eberly, S., Tanner, C.M., Oakes, D., Shoulson, I., and Huntington Study, G. (2009). Dietary intake in adults at risk for Huntington disease: analysis of PHAROS research participants. Neurology *73*, 385–392.

Markianos, M., Panas, M., Kalfakis, N., and Vassilopoulos, D. (2005). Plasma testosterone in male patients with Huntington's disease: relations to severity of illness and dementia. Ann. Neurol. *57*, 520–525.

Menalled, L., El-Khodor, B.F., Patry, M., Suarez-Farinas, M., Orenstein, S.J., Zahasky, B., Leahy, C., Wheeler, V., Yang, X.W., Macdonald, M., et al. (2009). Systematic behavioral evaluation of Huntington's disease transgenic and knock-in mouse models. Neurobiol. Dis. *35*, 319–336.

Meng, Q., and Cai, D. (2011). Defective hypothalamic autophagy directs the central pathogenesis of obesity via the IkappaB kinase beta (IKKbeta)/NF-kappaB pathway. J. Biol. Chem. *286*, 32324–32332.

Ochaba, J., Fote, G., Kachemov, M., Thein, S., Yeung, S.Y., Lau, A.L., Hernandez, S., Lim, R.G., Casale, M., Neel, M.J., et al. (2019). IKKbeta slows Huntington's disease progression in R6/1 mice. Proc. Natl. Acad. Sci. U S A *116*, 10952–10961.

Papalexi, E., Persson, A., Bjorkqvist, M., Petersen, A., Woodman, B., Bates, G.P., Sundler, F., Mulder, H., Brundin, P., and Popovic, N. (2005). Reduction of GnRH and infertility in the R6/2 mouse model of Huntington's disease. Eur. J. Neurosci. *22*, 1541–1546.

Pasparakis, M., Courtois, G., Hafner, M., Schmidt-Supprian, M., Nenci, A., Toksoy, A., Krampert, M., Goebeler, M., Gillitzer, R., Israel, A., et al. (2002). TNF-mediated inflammatory skin disease in mice with epidermis-specific deletion of IKK2. Nature *417*, 861–866.

Petersen, A., and Bjorkqvist, M. (2006). Hypothalamic-endocrine aspects in Huntington's disease. Eur. J. Neurosci. *24*, 961–967.

Petersen, A., Gil, J., Maat-Schieman, M.L., Bjorkqvist, M., Tanila, H., Araujo, I.M., Smith, R., Popovic, N., Wierup, N., Norlen, P., et al. (2005). Orexin loss in Huntington's disease. Hum. Mol. Genet. *14*, 39–47.

Pitteloud, N., Hardin, M., Dwyer, A.A., Valassi, E., Yialamas, M., Elahi, D., and Hayes, F.J. (2005). Increasing insulin resistance is associated with a decrease in Leydig cell testosterone secretion in men. J. Clin. Endocrinol. Metab. *90*, 2636–2641.

Politis, M., Pavese, N., Tai, Y.F., Tabrizi, S.J., Barker, R.A., and Piccini, P. (2008). Hypothalamic involvement in Huntington's disease: an in vivo PET study. Brain *131*, 2860–2869.

Pouladi, M.A., Stanek, L.M., Xie, Y., Franciosi, S., Southwell, A.L., Deng, Y., Butland, S., Zhang, W., Cheng, S.H., Shihabuddin, L.S., and Hayden, M.R. (2012). Marked differences in neurochemistry and aggregates despite similar behavioural and neuropathological features of Huntington disease in the full-length BACHD and YAC128 mice. Hum. Mol. Genet. *21*, 2219–2232.

Pouladi, M.A., Xie, Y., Skotte, N.H., Ehrnhoefer, D.E., Graham, R.K., Kim, J.E., Bissada, N., Yang, X.W., Paganetti, P., Friedlander, R.M., et al. (2010). Full-length huntingtin levels modulate body weight by influencing insulin-like growth factor 1 expression. Hum.Mol.Genet. *19*, 1528–1538.

Procaccini, C., Santopaolo, M., Faicchia, D., Colamatteo, A., Formisano, L., De Candia, P., Galgani, M., De Rosa, V., and Matarese, G. (2016). Role of metabolism in neurodegenerative disorders. Metabolism *65*, 1376–1390.

Saleh, N., Moutereau, S., Durr, A., Krystkowiak, P., Azulay, J.P., Tranchant, C., Broussolle, E., Morin, F., Bachoud-Levi, A.C., and Maison, P. (2009). Neuroendocrine disturbances in Huntington's disease. PLoS One *4*, e4962.

Sarkar, S., Korolchuk, V.I., Renna, M., Imarisio, S., Fleming, A., Williams, A., Garcia-Arencibia, M., Rose, C., Luo, S., Underwood, B.R., et al. (2011). Complex inhibitory effects of nitric oxide on autophagy. Mol.Cell *43*, 19–32.

Shi, Y.C., Lau, J., Lin, Z., Zhang, H., Zhai, L., Sperk, G., Heilbronn, R., Mietzsch, M., Weger, S., Huang, X.F., et al. (2013). Arcuate NPY controls sympathetic output and BAT function via a relay of tyrosine hydroxylase neurons in the PVN. Cell Metab. *17*, 236–248.

Sjogren, M., Soylu-Kucharz, R., Dandunna, U., Stan, T.L., Cavalera, M., Sandelius, A., Zetterberg, H., and Bjorkqvist, M. (2019). Leptin deficiency reverses high metabolic state and weight loss without affecting central pathology in the R6/2 mouse model of Huntington's disease. Neurobiol. Dis. *132*, 104560.

Soneson, C., Fontes, M., Zhou, Y., Denisov, V., Paulsen, J.S., Kirik, D., Petersen, A., and Huntington Study Group PREDICT-HD investigators. (2010). Early changes in the hypothalamic region in prodromal Huntington disease revealed by MRI analysis. Neurobiol. Dis. *40*, 531–543.

Soylu-Kucharz, R., Adlesic, N., Baldo, B., Kirik, D., and Petersen, A. (2015). Hypothalamic overexpression of mutant huntingtin causes dysregulation of brown adipose tissue. Sci. Rep. *5*, 14598.

Soylu-Kucharz, R., Adlesic, N., Henningsen, J., Davidsson, M., Bjorklund, T., Björkqvist, M., and Petersén, Å. (2018). A53 Effects of hypothalamic circuitries on pathology in the ventral striatum in mouse models of huntington disease. J. Neurol. Neurosurg. Psychiatry *89*, A19.

Soylu-Kucharz, R., Baldo, B., and Petersen, A. (2016). Metabolic and behavioral effects of mutant huntingtin deletion in Sim1 neurons in the BACHD mouse model of Huntington's disease. Sci. Rep. *6*, 28322.

Thompson, L.M., Aiken, C.T., Kaltenbach, L.S., Agrawal, N., Illes, K., Khoshnan, A., Martinez-Vincente, M., Arrasate, M., O'rourke, J.G., Khashwji, H., et al. (2009). IKK phosphorylates Huntingtin and targets it for degradation by the proteasome and lysosome. J. Cell Biol. *187*, 1083–1099.

Timper, K., and Bruning, J.C. (2017). Hypothalamic circuits regulating appetite and energy homeostasis: pathways to obesity. Dis. Model. Mech. *10*, 679–689.

Trager, U., Andre, R., Lahiri, N., Magnusson-Lind, A., Weiss, A., Grueninger, S., Mckinnon, C., Sirinathsinghji, E., Kahlon, S., Pfister, E.L., et al. (2014). HTT-lowering reverses Huntington's disease immune dysfunction caused by NFkappaB pathway dysregulation. Brain *137*, 819–833.

van der Burg, J.M.M., Gardiner, S.L., Ludolph, A.C., Landwehrmeyer, G.B., Roos, R.A.C., and Aziz, N.A. (2017). Body weight is a robust predictor of clinical progression in Huntington disease. Ann. Neurol. *82*, 479–483.

Van Raamsdonk, J.M., Metzler, M., Slow, E., Pearson, J., Schwab, C., Carroll, J., Graham, R.K., Leavitt, B.R., and Hayden, M.R. (2007a). Phenotypic abnormalities in the YAC128 mouse model of Huntington disease are penetrant on multiple genetic backgrounds and modulated by strain. Neurobiol. Dis. *26*, 189–200.

Van Raamsdonk, J.M., Murphy, Z., Selva, D.M., Hamidizadeh, R., Pearson, J., Petersen, A., Bjorkqvist, M., Muir, C., Mackenzie, I.R., et al. (2007b). Testicular degeneration in Huntington disease. Neurobiol. Dis. *26*, 512–520.

Walker, F.O., and Raymond, L.A. (2004). Targeting energy metabolism in Huntington's disease. Lancet *364*, 312–313.

West, M.J., Slomianka, L., and Gundersen, H.J. (1991). Unbiased stereological estimation of the total number of neurons in thesubdivisions of the rat hippocampus using the optical fractionator. Anatomical Rec. *231*, 482–497.

Zhang, G., Li, J., Purkayastha, S., Tang, Y., Zhang, H., Yin, Y., Li, B., Liu, G., and Cai, D. (2013). Hypothalamic programming of systemic ageing involving IKK-beta, NF-kappaB and GnRH. Nature *497*, 211–216.

Zhang, X., Zhang, G., Zhang, H., Karin, M., Bai, H., and Cai, D. (2008). Hypothalamic IKKbeta/NF-kappaB and ER stress link overnutrition to energy imbalance and obesity. Cell *135*, 61–73.

Zhang, Y., Reichel, J.M., Han, C., Zuniga-Hertz, J.P., and Cai, D. (2017). Astrocytic process plasticity and IKKbeta/NF-kappaB in central control of blood glucose, blood pressure, and body weight. Cell Metab. *25*, 1091–1102 e4.

Zielonka, D., Marinus, J., Roos, R.A., De Michele, G., Di Donato, S., Putter, H., Marcinkowski, J., Squitieri, F., Bentivoglio, A.R., and Landwehrmeyer, G.B. (2013). The influence of gender on phenotype and disease progression in patients with Huntington's disease. Parkinsonism Relat. Disord. *19*, 192–197.

Zielonka, D., Ren, M., De Michele, G., Roos, R.A.C., Squitieri, F., Bentivoglio, A.R., Marcinkowski, J.T., and Landwehrmeyer, G.B. (2018). The contribution of gender differences in motor, behavioral and cognitive features to functional capacity, independence and quality of life in patients with Huntington's disease. Parkinsonism Relat. Disord. *49*, 42–47.

Zielonka, D., and Stawinska-Witoszynska, B. (2020). Gender differences in non-sex linked disorders: insights from huntington's disease. Front. Neurol. *11*, 571.

STAR★METHODS

KEY RESOURCES TABLE

REAGENT or RESOURCE	SOURCE	IDENTIFIER
Antibodies		
anti-huntingtin	Santa Cruz	RRID:AB_2123254
anti-ubiquitin	Dako	RRID:AB_2315524
anti-orexin	Phoenix Pharmaceuticals	RRID:AB_2315019
anti-tyrosine hydroxylase	Pel-Freez	RRID:AB_461064
anti-GnRH	Abcam	Cat# ab5617, RRID:AB_304986
anti-iba-1	Wako	RRID:AB_839504
Bacterial and virus strains		
rAAV2/5-853HTT-79Q	Lund University Virus Production (Hult et al., 2011)	N/A
Chemicals, peptides, and recombinant proteins		
Trizma® base	Sigma-Aldrich	Cat# T6066
NaCl	Sigma-Aldrich	Cat# P3756
Triton-x	Sigma-Aldrich	Cat# T9284
Na2HPO4	Sigma-Aldrich	Cat# 1.06580.1000
NaH2PO4	Merck	Cat# 106346
Ethylene glycol ≥98%	VWR	Cat# 24407.361
Glycerol	VWR	Cat# 24387.361
Methanol	Sigma-Aldrich	Cat# 34860-251
H2O2 30%	Merck	Cat# 1.07209
Ethanol 70%	VWR	Cat# 83.801.360
Ethanol 95%	VWR	Cat# 20824.365
Ethanol Abs	VWR	Cat# 208.21
Xylen	VWR	Cat# 28973.363
Cover glass 24 × 60 mm # 1	VWR	Cat# 631-1339
DPX	Sigma-Aldrich	Cat# 1.00579.500
Horse Serum	Gibco	Cat# 16050130
Goat Serum	Gibco	Cat# 16210064
3-30 diaminobenzidine tetrahydrochloride	Saveen Werner AB	Cat# DAB25
VECTASTAIN Elite ABC-HRP Kit	Vector Laboratories	Cat# PK-6100
Chromium (III) Potassium Sulfate Dodecahydrate, ≥98%	Sigma-Aldrich	Cat# 243361
Pentobarbitalnatrium	Apoteket	Cat# 338327
Isoflurane (IsoFlo vet. 100%)	Apoteket	Cat#002185
Critical commercial assays		
Insulin ELISA	Crystal Chem Inc.	Cat #90080
Leptin ELISA	Crystal Chem Inc.	Cat #90030
Testosterone ELISA	Demeditec	Cat #DEV9911
Experimental models: Organisms/strains		
IKKβ$^{lox/lox}$	Michael Karin university of San Diego California (Li et al., 2003)	N/A
B6.Cg-Tg(Nes-cre)1Kln/J	The Jackson Laboratory	Cat# Jax:003771

(*Continued on next page*)

Continued

REAGENT or RESOURCE	SOURCE	IDENTIFIER
Oligonucleotides		
Forward primer for IKKβ$^{lox/lox}$ and Nestin/IKKβ$^{lox/lox}$ alleles 5′-GTC ATT TCC ACA GCC CTG TGA-3′	(Li et al., 2003)	N/A
Reverse primer for IKKβ$^{lox/lox}$ and Nestin/IKKβ$^{lox/lox}$ alleles 5′-CCT TGT CCT ATA GAA GCA CAA C-3′	(Li et al., 2003)	N/A
Forward primer for Cre genotype 5′-GCG GTC TGG CAG TAA AAA CTA TC-3′	The Jackson Laboratory	oIMR1084
Reverse primer for Cre genotype 5′-GTG AAA CAG CAT TGC TGT CAC TT-3′	The Jackson Laboratory	oIMR1085
Software and algorithms		
Prism 8 software (V8.4.3)	GraphPad	https://www.graphpad.com
Stereology software	Visiopharm	https://visiopharm.com/
Other		
Micropipette Glass	Stoelting	Cat# 50811
Hamilton syringe 5ul	VWR	Cat# 549-1231

RESOURCE AVAILABILITY

Lead contact

Further information and requests for resources and reagents should be directed to and will be fulfilled by the lead contact, Rana Soylu-Kucharz, rana.soylu_kucharz@med.lu.se.

Materials availability

This study did not generate new unique reagents.

Data and code availability

- All data reported in this paper will be shared by the lead contact upon request.
- This paper does not report original code.
- Any additional information required to reanalyze the data reported in this paper is available from the lead contact upon request.

EXPERIMENTAL MODEL AND SUBJECT DETAILS

Animals

The experimental procedures performed on mice were carried out using the approved guidelines in the ethical permit approved by the Lund University Animal Welfare and Ethics committee in the Lund-Malmö region (ethical permit numbers M20–11 and M65-13). To silence the function of IKKβ in neuronal tissue, we crossed mice from C57BL background strain, carrying a loxP-site-flankingIKKβ allele (IKKβ$^{lox/lox}$) (Pasparakis et al., 2002) with mice heterozygous for Cre recombinase gene carrying the loxP-site-flankedIKKβ allele (Nestin/IKKβ$^{lox/lox}$). Cre recombinase deletes exons 6 and 7 of the IKKβ coding DNA sequence under nestin promoter,producing premature termination codons resulting in an IKKβ null allele in nestin-expressing cells. Generation of IKKβ$^{lox/lox}$ mice (Li et al., 2003) and Nestin-Cre mice (Betz et al., 1996) was described previously. Nestin/IKKβ$^{lox/lox}$ mice were generated following several generations of backcrossing. In this study, we crossed the IKKβ$^{lox/lox}$ with mice Nestin/IKKβ$^{lox/lox}$ heterozygous for Cre-recombinase gene. The development of IKKβ$^{lox/lox}$ is similar to wild-type mice and expresses normal levels of IKKβ (Pasparakis et al., 2002). The experiments were carried out on 2–6 months old mice, both male and female mice, with the genotypes of Nestin/IKKβ$^{lox/lox}$ mice and their IKKβ$^{lox/lox}$ WT littermates. The age of the mice before the surgery was distributed equally between the genotypes in females (two-tailed Mann-Whitney test: p = 0.917, IKKβ$^{lox/lox}$ Mean = 21.51 weeks old, SD = 5.183, SEM = 1.338; Nestin/IKKβ$^{lox/lox}$ Mean = 20.95 weeks old, SD = 6.363, SEM = 1.389 and in males (two-tailed Mann-Whitney test: p = 0.2133, IKKβ$^{lox/lox}$ Mean = 18.36 weeks old, SD = 7.127, SD = 1.594; Nestin/IKKβlox/lox Mean = 20.84 weeks old, SD = 6.481,

SEM = 1.382). The age of the mice was also distributed equally between the genders (Kruskal-Wallis test followed by Dunn's multiple comparisons, p = 0.4046; n = 15-22/group). The animals were kept in a controlled environment at 22°C with 12 h night/day cycle and had free access to a standard chow diet and water throughout the study. Genotyping was performed using the following primer sequences that amplify both the IKKβ$^{lox/lox}$ (220-bp) and Nestin/IKKβ$^{lox/lox}$ (310-bp) alleles 5'-GTC ATT TCC ACA GCC CTG TGA-3' and 5'-CCT TGT CCT ATA GAA GCA CAA C-3' and for the determination of Nestin-Cre genotype 5'-GCG GTC TGG CAG TAA AAA CTA TC-3' and 5'-GTG AAA CAG CAT TGC TGT CAC TT-3' primers were used (Chen et al., 2003, Li et al., 2003).

Adeno-associated viral vectors

To investigate the effect of the IKK pathway on the development of the mHTT-mediated metabolic phenotype, we performed stereotactic injections of recombinant adeno-associated viral (rAAV) vectors into the hypothalamus of IKKβ$^{lox/lox}$ and Nestin/IKKβ$^{lox/lox}$ mice. The viral vector was a pseudotyped rAAV2/5 vector (transgene was flanked by two inverted terminal repeats of the AAV2 and packaged in an AAV5 capsid), expressing N-terminal fragment of 853 amino acids length (853HTT79Q) human mHTT (Hult et al., 2011). The human Synapsin-1 promoter drove the mHTT gene expression.

METHOD DETAILS

Viral vector injections

The animals were anesthetized by air mask inhalation of isoflurane (2% isoflurane in O2/N2O (3:7)). The mouse head was fixed with a nose clamp and ear bars in the stereotaxic apparatus. Following the head position's fine-tuning on the stereotaxic frame, the skull was thinned with a dental drill to make a borehole at the determined anterior-posterior and medial-lateral hypothalamic coordinates. Subsequently, the final dorsal-ventral coordinates were measured from the dura mater. The stereotaxic coordinates chosen for hypothalamic injections were: 0.6 mm posterior to bregma, −0.6 mm lateral to the bregma, and 5.2 mm ventral to the dura mater, selected according to the mouse brain atlas (Franklin and Paxinos, 2008).

The rAAV vector delivery was performed bilaterally in the hypothalamus. The silica glass capillary (with an outer diameter of ~80 μm) attached to a 5 μl Hamilton syringe (Nevada, USA) was used for the virus delivery. A total volume of 0.5 μl viral vector solution was pulled in a glass capillary, and the capillary was descended from the dura mater to target coordinates slowly. At the target, the first 0.1 μl of the total volume was injected. After 30 s, the viral suspension was delivered at a rate of 0.05μl/15s until the whole volume was delivered. To allow the brain to absorb the viral vector solution, the capillary was left at the target for an additional 5 min at the end of the injection. The viral vector concentration used in the study was 2,1E+14 genome copies (GC)/ml.

Perfusion and serum collection

To induce deep anesthesia in mice, a terminal dose of pentobarbital (600 mg/kg, Apoteksbolaget) was injected intraperitoneally. The thoracic cavity was opened to expose the heart, and blood was collected from the right ventricle with the 16G needle. Subsequently, a small incision was made to insert a 12-gauge perfusion needle at the tip of the left ventricle. First, the vessels were rinsed with the saline solution at a rate of 10-12 ml/min for a minute, and then it was switched to freshly prepared 4% paraformaldehyde (PFA) ~0°C for 8 min. Following that, the animals were decapitated, and the brains were isolated. The brains were placed in 4% PFA for 24 h at 4°C for post-fixation. Next, the PFA was replaced with 25% sucrose solution at 4°C for cryoprotection (~24 h). Finally, the fixed brains were sectioned coronally on a semi-automated freezing microtome (Microm HM 450) at 30 μm thick slices and in six series. Until further processing, the brain sections were stored in antifreeze solution (30% glycerol and 30% ethylene glycol in phosphate buffer) at −20°C.

Metabolic tests

For all animals used in the study, body weight was measured bimonthly. Serum insulin and leptin concentrations were assessed in serum. Blood was collected from the heart left ventricle at 18 weeks post-injection, and they were kept at room temperature for 30 min to clot, spun for 15 min at 2500 g. Serum (supernatant) was aliquoted and stored at −80 C. Serum levels of insulin (Crystal Chem Inc, Cat #90080), leptin (Crystal Chem Inc, Cat #90030) and testosterone (Demeditec, Cat #DEV9911) were determined with ELISA according to the manufacturer's instructions.

Immunohistochemistry

The free-floating brain sections were used for immunohistochemistry (IHC). All the washing steps (10 min/wash) and incubations were performed using gentle agitation on a shaker at room temperature. The sections were washed three times in Tris-buffered saline (TBS) in 1% Triton X-(TBS-T) to remove the antifreeze solution. The endogenous peroxidase activity was blocked by 30 min of incubation in 10% methanol with 3% H2O2 in TBS. Following that, the sections were washed three times for 10 min in TBS-T. The sections were incubated with 5% serum and bovine serum albumin (BSA) in TBS-T for 1 h to reduce nonspecific binding of the primary and secondary antibodies. Next, the sections were left in the respective primary antibody solutions in 3% appropriate corresponding serum in TBS-T (anti-huntingtin (sc-8767; 1:500; goat; Santa Cruz, RRID:AB_2123254), anti-ubiquitin (1:2000; rabbit; Dako, RRID:AB_2315524), anti-orexin (1:4000; rabbit; Phoenix Pharmaceuticals, RRID:AB_2315019), anti-tyrosine hydroxylase (1:2000; rabbit; Pel-Freez, RRID:AB_461064), anti-GnRH (1:3000, anti-rabbit, Abcam #ab5617, RRID:AB_304986), anti-iba-1 (1:1000, rabbit, Wako, RRID:AB_839504) and left on shaker for overnight incubation at room temperature. Next, sections were washed three times for 10 min in TBS-T. The secondary antibody incubation was performed in 3% respective serum or BSA with TBS-T for 1 h at room temperature, and the sections were washed three times for 10 min in TBS before 3,3′-diaminobenzidine (DAB) development (Vectastain, ABC kit). Brain sections were mounted on chromatin-gelatin-coated glass slides. The air-dried sections were left in distilled water for 1 min and dehydrated in increasing ethanol solutions (70%, 95%, 99%). Finally, the samples were cleared in xylene and covered with glass coverslips using DPX mounting medium (Sigma-Aldrich).

Stereological analyses

To estimate the numbers of cells positive for orexin, TH, GnRH (in the anterior hypothalamus; AHA), and size of the inclusions, we applied unbiased stereological quantification principles by using the optical dissector method (West et al., 1991). Stereological analyses were performed with a Nikon 80i microscope, which is equipped with an X–Y motorized stage (Märzhauser, Wetzlar) and a high precision linear encoder (Heidenhain, Traunreut). The position of the stage and the input from the digital camera were controlled by a computer. The sampling interval was adjusted to count at least 100 cells for each hypothalamus to minimize the coefficient of error. The region of interest was delineated under the 4X objective, whereas the counting was performed using a 60X NA 1.4 Plan-Apo oil objective with a random start systematic sampling routine (NewCast Module in VIS software; Visiopharm A/S, Horsholm). The border delineation processes for orexin, TH, GnRH cell populations were defined by the natural contours of cell populations. The number and size of iba-1 positive microglia/macrophages were quantified in the anatomical borders of the medi-obasal hypothalamus. The number of small, medium and large size HTT inclusions was quantified with HTT staining (sc-6787). The inclusions ~0.04–0.1 μm size considered small, 0.15–0.25 μm medium and ~0.25–0.5 μm large size inclusions. The same size of the region of interest was quantified for all genotypes and gender under blinded conditions. The mean number of assessed inclusions per brain was 755, median 663 with a standard deviation of error 528 inclusions. The mean crossectional area for iba1-positive cells and mutant HTT inclusions were quantified by applying the nucleator probe using a 60X NA 1.4 Plan-Apo oil objective and unbiased stereological quantification principles (NewCast Module in VIS software; Visiopharm A/S, Horsholm) (Gundersen et al., 1988).

QUANTIFICATION AND STATISTICAL ANALYSIS

All statistical analyses were performed using Prism 8 software (GraphPad). The data was initially tested with D'Agostino & Pearson omnibus normality test for normal distribution. Following that, the data was either subjected to Kruskal-Wallis followed by Dunn's multiple comparison tests or an unpaired t-test with equal SD. The statistical test results and the type of analysis used for each experiment are specified in detail in the results section and figure legends. Statistically significant differences were considered for $p<0.05$ and exact $p<0.0001$ values are reported in Table S1.